

Supporting Information for

Pyrene-Based Covalent Organic Polymers with Nano Carbonaceous Composites for Efficient Supercapacitive Energy Storage

Mohsin Ejaz,^{a#} Mohamed Gamal Mohamed,^{a,b,#,*} Wei-Chun Huang,^a and Shiao-Wei Kuo^{a,c*}

^a Department of Materials and Optoelectronic Science, College of Semiconductor and Advanced Technology Research, Center of Crystal Research, National Sun Yat-Sen University, Kaohsiung 804, Taiwan.

^b Chemistry Department, Faculty of Science, Assiut University, Assiut 71515, Egypt.

^c Department of Medicinal and Applied Chemistry, Kaohsiung Medical University, Kaohsiung 807, Taiwan.

* Correspondence: mgamal.eldin12@yahoo.com (M. G. Mohamed); kuosw@faculty.nsysu.edu.tw (S. W. Kuo)

These authors equally contributed.

Characterization

FTIR spectra were collected using a Bruker Tensor 27 FTIR spectrophotometer at 4 cm^{-1} resolution and the KBr disk method. ^{13}C nuclear magnetic resonance (NMR) spectra were recorded using an INOVA 500 instrument, with DMSO as the solvent and tetramethylsilane (TMS) as the external standard; chemical shifts are reported in parts per million (ppm). The thermal stabilities of the samples under N_2 were measured using a TG Q-50 thermogravimetric analyzer; the cured sample (ca. 5 mg) was placed in a Pt cell and then heated at $20\text{ }^\circ\text{C min}^{-1}$ from 100 to $800\text{ }^\circ\text{C}$ under a N_2 flow of 60 mL min^{-1} . Wide-angle X-ray diffraction (WAXD) patterns were measured at the wiggler beamline BL17A1 of the National Synchrotron Radiation Research Center (NSRRC), Taiwan; a triangular bent Si (111) single crystal was used to obtain a monochromated beam having a wavelength (λ) of 1.33 \AA . The morphologies of the polymer samples were examined through field emission scanning electron microscopy (FE-SEM; JEOL JSM7610F) and transmission electron microscopy (TEM), using a JEOL-2100 microscope operated at an accelerating voltage of 200 kV. BET surface areas and porosimetry measurements of the samples (ca. 40–100 mg) were performed using a BEL MasterTM instrument and BEL simTM software (v. 3.0.0); N_2 adsorption and desorption isotherms were generated through incremental exposure to ultrahigh-purity N_2 (up to ca. 1 atm) in a liquid N_2 (77 K) bath; surface parameters were calculated using the BET adsorption models in the instrument's software. The pore sizes of the prepared samples were determined using nonlocal density functional theory (NLDFT).

Electrochemical Analysis

Working Electrode Cleaning: Prior to use, the glassy carbon electrode (GCE) was polished several times with $0.05\text{-}\mu\text{m}$ alumina powder, washed with EtOH after each polishing step, cleaned through sonication (5 min) in a water bath, washed with EtOH, and then dried in air.

Electrochemical Characterization: The electrochemical experiments were performed in a three-electrode cell using an Autolab potentiostat (PGSTAT204) and 1 M KOH as the aqueous electrolyte.

The GCE was used as the working electrode (diameter: 5.61 mm; 0.2475 cm²); a Pt wire was used as the counter electrode; Hg/HgO (RE-1B, BAS) was the reference electrode. All reported potentials refer to the Hg/HgO potential. A slurry was prepared by dispersing the Py-DSDA-COP or Py-DSDA-COP/C60 or Py-DSDA-COP/MWCNTs or Py-DSDA-COP/SWCNTs samples (2 mg), carbon black (2 mg), and Nafion (10 wt. %) in a mixture of (EtOH/ H₂O) (200 μL: 800 μL) and then sonicated for 1 h. A portion of this slurry (5 μL) was pipetted onto the tip of the electrode, which was then dried in air for 30 min prior to use. The electrochemical performance was studied through CV at various sweep rates (5–200 mV s⁻¹) and through the GCD method in the potential range from 0 to –1.00 V (vs. Hg/HgO) at various current densities (0.5–20 A g⁻¹) in 1 M KOH as the aqueous electrolyte solution.

The specific capacitance was calculated from the GCD data using the equation:

$$C_s = (I\Delta t)/(m\Delta V) \quad (\text{S1})$$

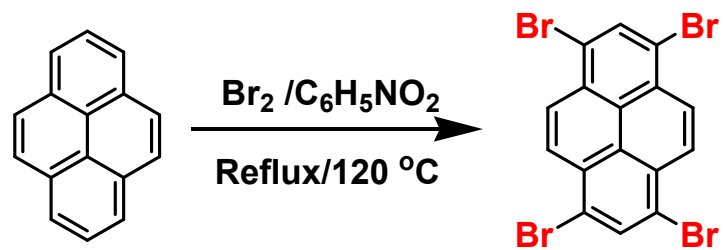
Where C_s (F g⁻¹) is the specific capacitance of the supercapacitor, I (A) is the discharge current, ΔV (V) is the potential window, Δt (s) is the discharge time, and m (g) is the mass of the NPC on the electrode. The energy density (E , W h kg⁻¹) and power density (P , W kg⁻¹) were calculated using the equations.

$$E = 1000C(\Delta V)^2/(2 \times 3600) \quad (\text{S2})$$

$$P = E/(t/3600) \quad (\text{S3})$$

We evaluated the electrochemical functionality of a symmetric supercapacitor using a CR2032 coin cell, which consists of an anode and cathode, a bottom and top cover, a metal spring, a separator, and an electrolyte. Our compounds served as both the cathode and the anode in order to construct a symmetric supercapacitor. The slurry was created by combining 2 mg of Py-DSDA-COP or Py-DSDA-COP/C60 or Py-DSDA-COP/MWCNTs or Py-DSDA-COP/SWCNTs, 2 mg of conductive carbon, 20 μL of nafion, 200 μL of ethanol, and 400 μL of water. It was then sonicated for an hour and cast onto carbon paper. We used a Selemion AMV membrane with an electrolyte of 1.0 M

aqueous KOH. The thickness of the electrodes was 0.08 cm for each electrode. The specific capacitance was calculated in assembled supercapacitor from the GCD data using the following equations: $C_s = 2(I\Delta t)/(m\Delta V)$ where C_s ($F\ g^{-1}$) is the specific capacitance of the supercapacitor, I (A) is the discharge current, ΔV (V) is the potential window, Δt (s) is the discharge time, and m (g) is the mass of the Py-COP the in the single electrode.



Scheme S1. Synthesis of Py-Br₄.

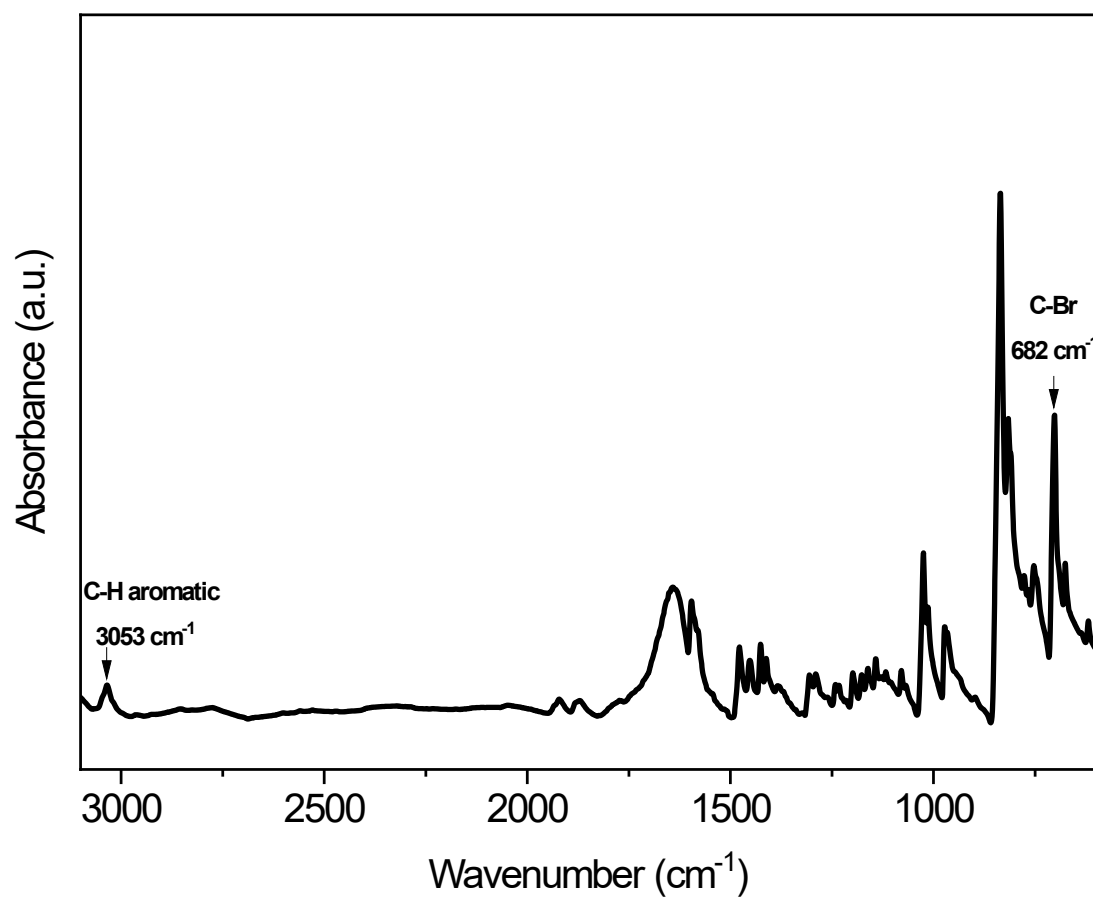


Figure S1. FT-IR spectrum of Py-Br₄.

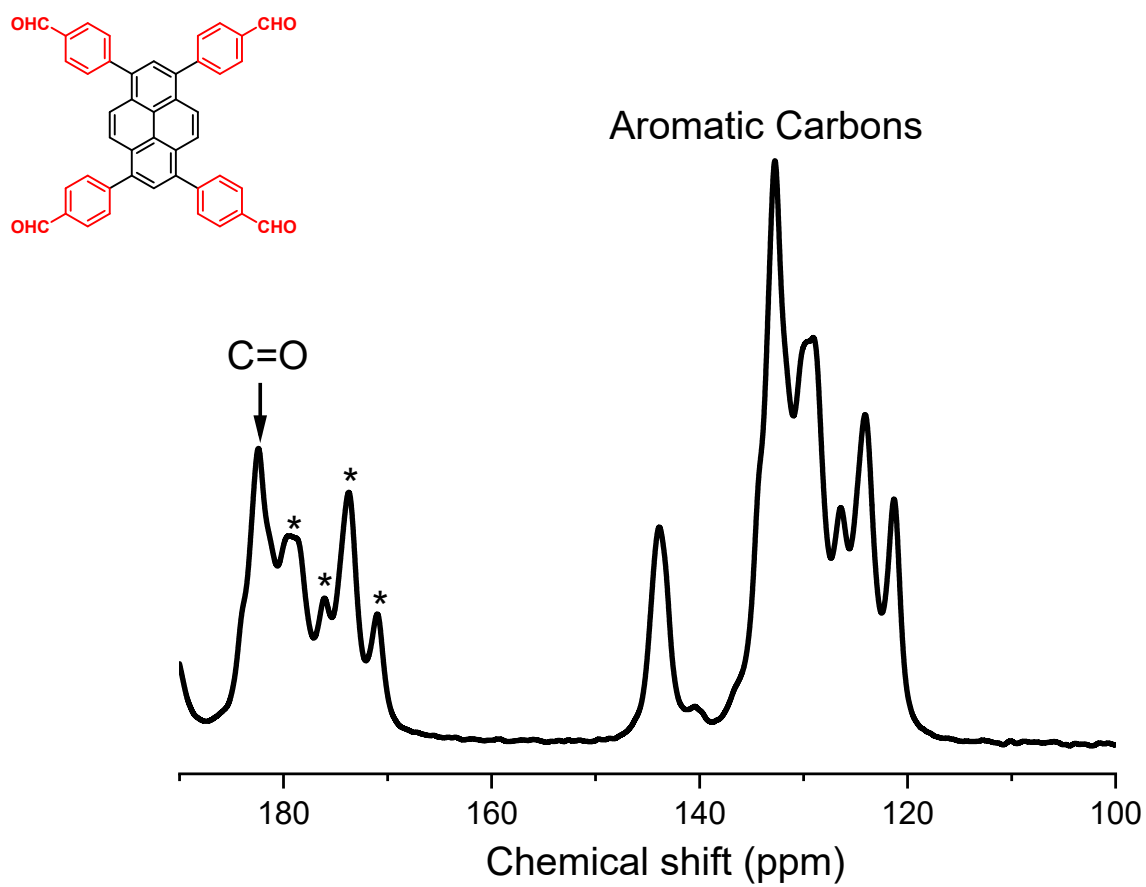


Figure S2. Solid state NMR spectrum of Py-Ph-CHO.

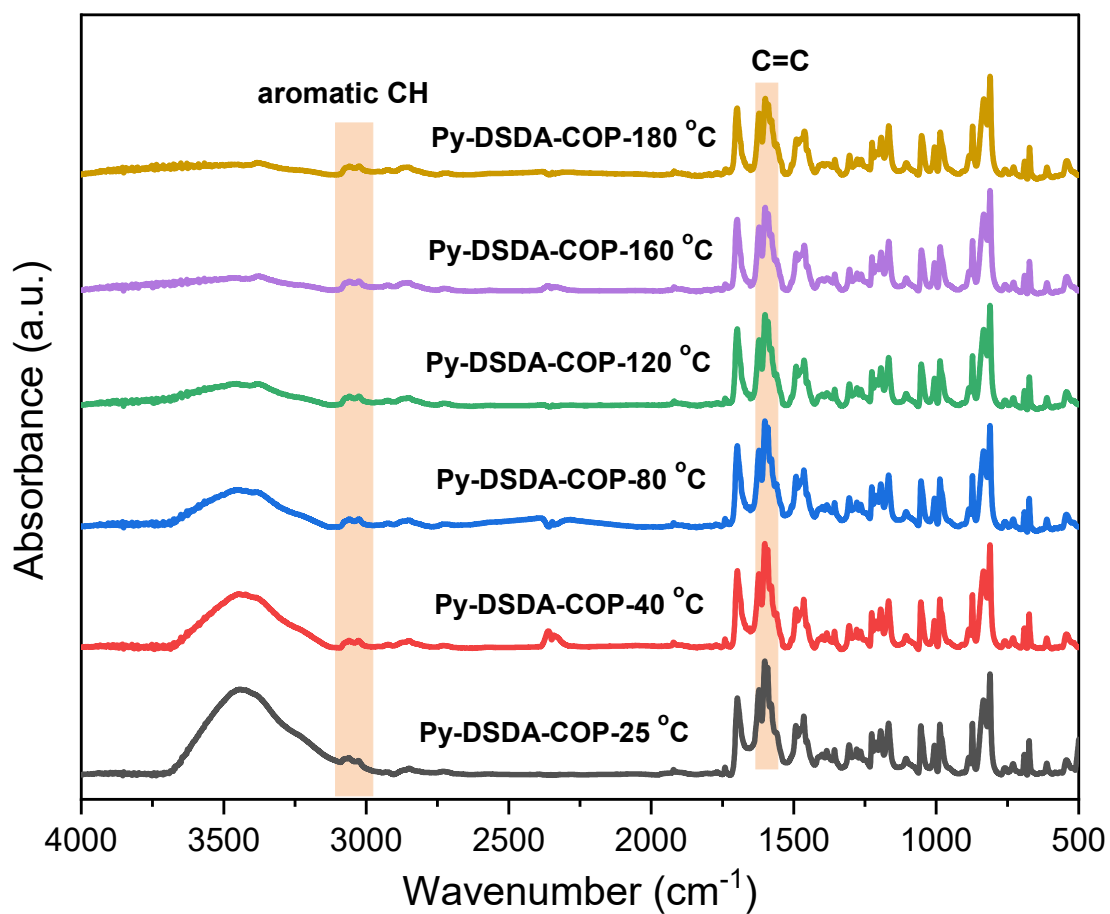


Figure S3. FTIR profiles of Py-DSDA-COP (recorded at different temperatures from 25 to 180 °C).

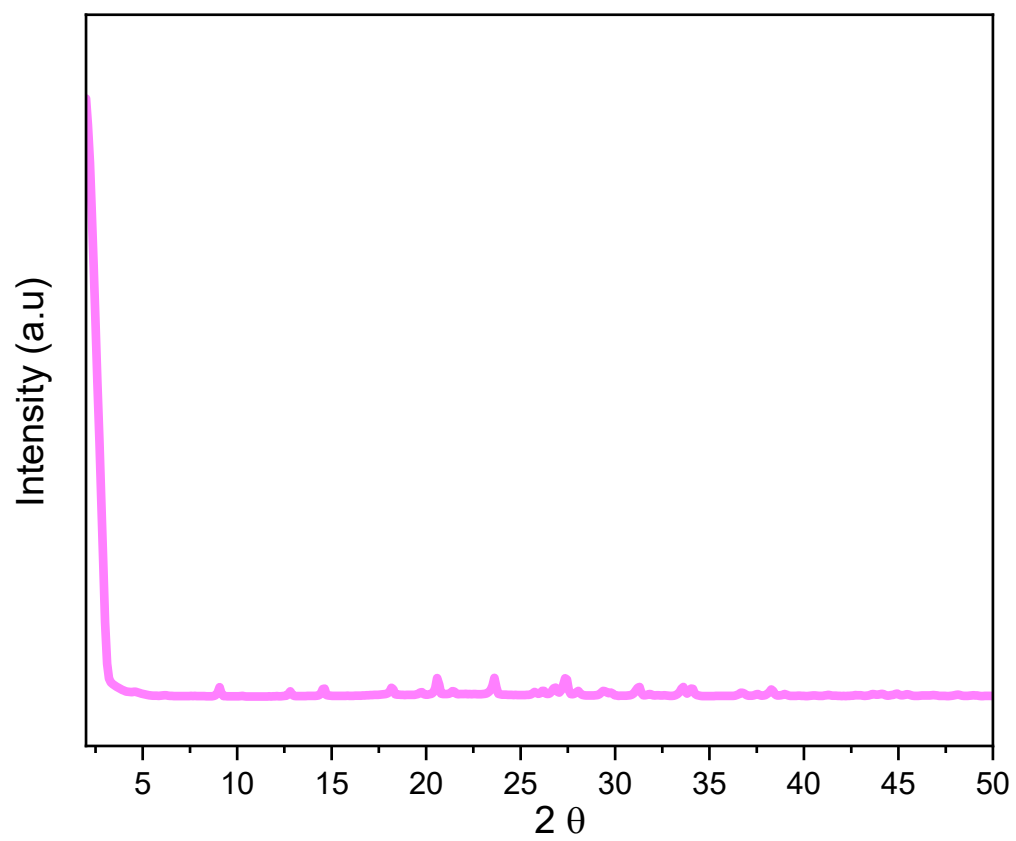


Figure S4. X-ray diffraction (XRD) pattern of Py-DSDA-COP material.

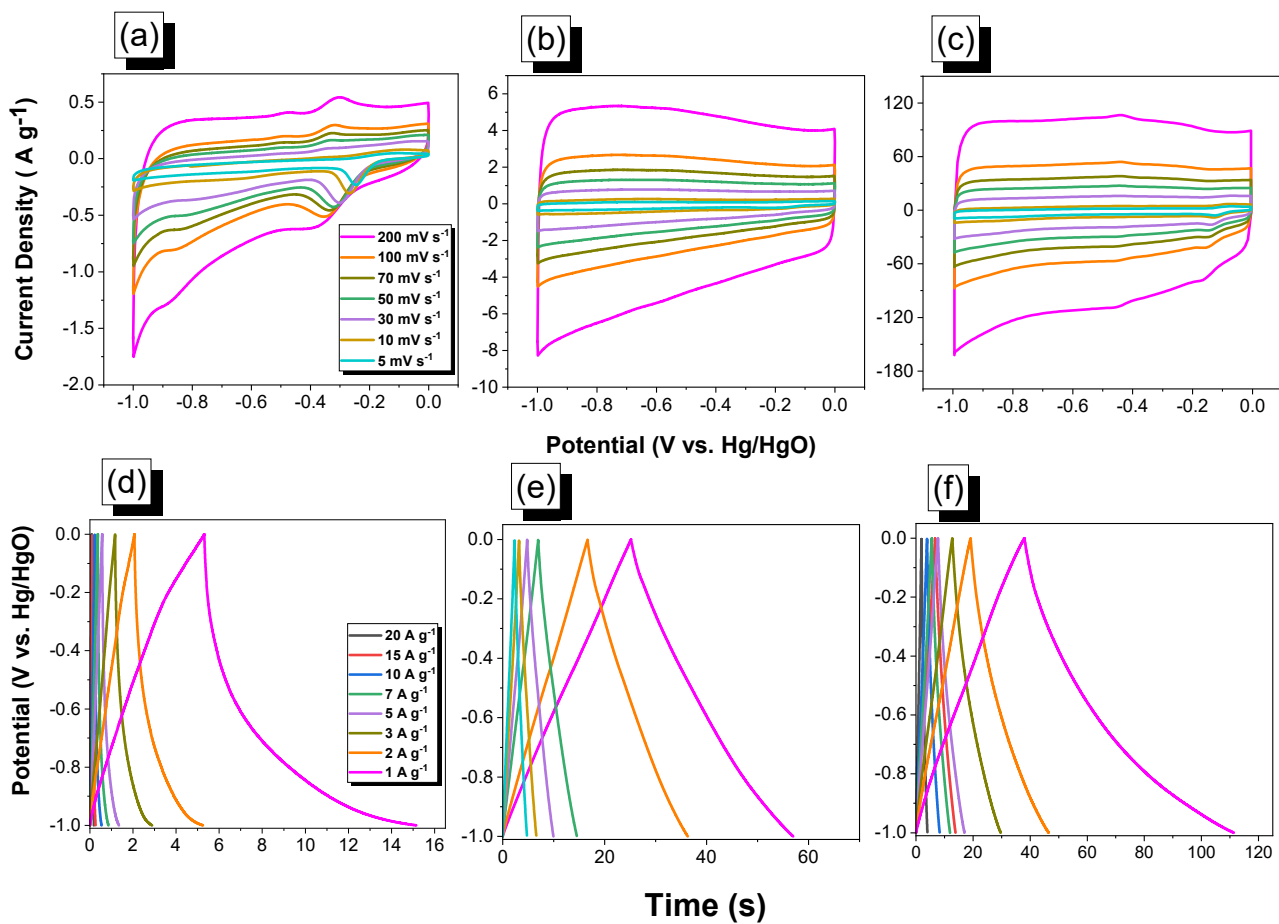


Figure S5. CV curves of (a) C60, (b) MWCNTs, and (c) SWCNTs. GCD curves of (d) C60, (e) MWCNTs, and (f) SWCNTs.

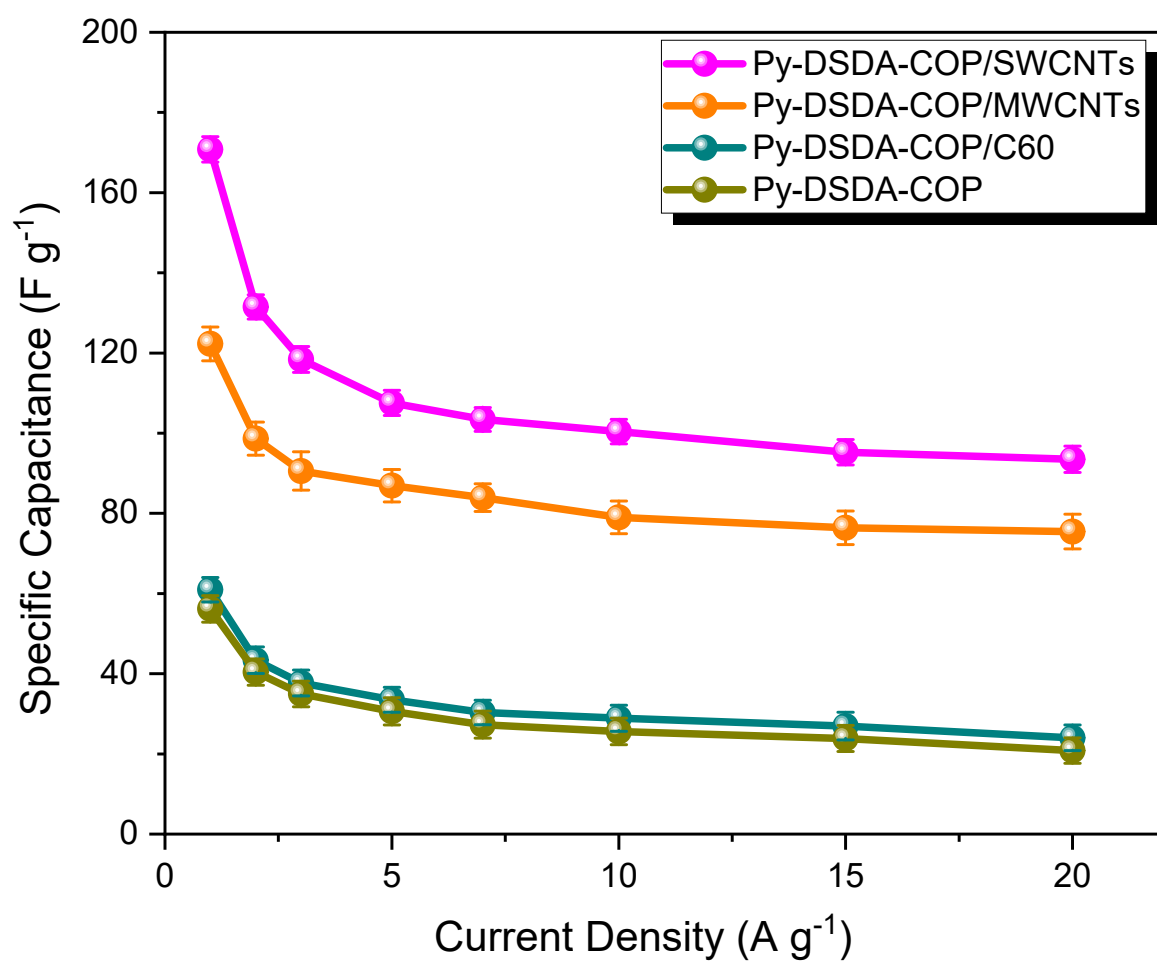


Figure S6. The specific capacitance of Py-DSDA-COP and their nanocomposite with error bars.

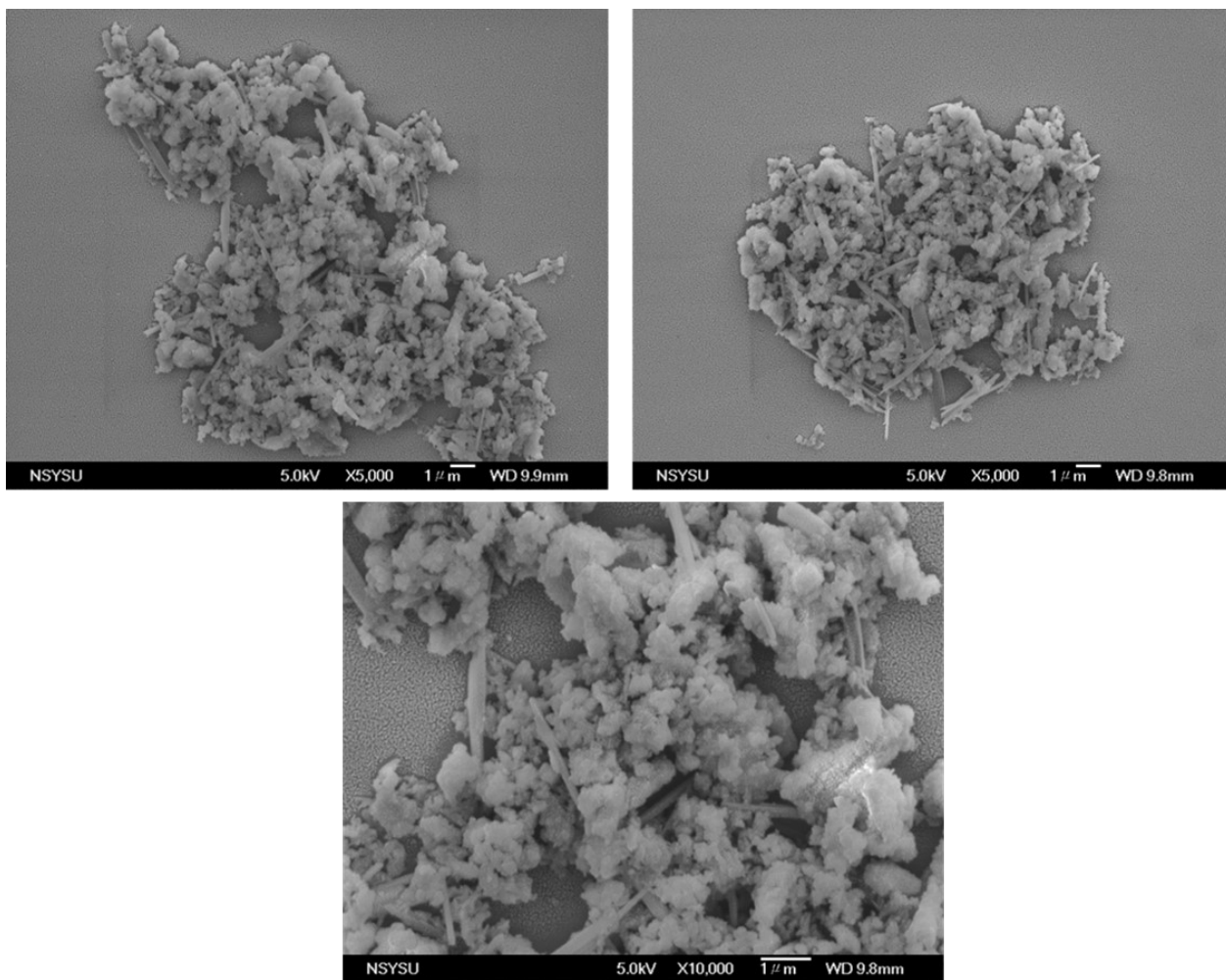


Figure S7. SEM images of Py-DSDA-COP after electrochemical analyses.

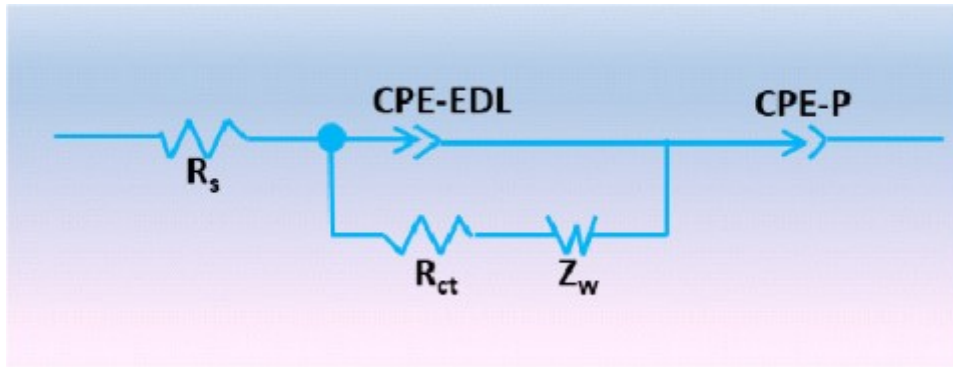


Figure S8. Equivalent fitted circuit to determine series resistance (R_s) and charge transfer resistance (R_{ct}).

Table S1. Comparison between the specific capacitance Py-DSDA-COP and Py-DSDA-COP/nanocomposites with those of previously reported materials for supercapacitor application.

Electrode	Capacitance	Ref.
Py-DSDA-COP	56.18 F g ⁻¹ at 1 A g ⁻¹	This work
Py-DSDA-COP/C60	60.96 F g ⁻¹ at 1 A g ⁻¹	This work
Py-DSDA-COP/MWCNTs	122.27 F g ⁻¹ at 1 A g ⁻¹	This work
Py-DSDA-COP/SWCNTs	170.8 F g ⁻¹ at 1 A g ⁻¹	This work
TBN-Py-CMP	31 F g ⁻¹ at 0.5 A g ⁻¹	S1
TBN-TPE-CMP	18.45 F g ⁻¹ at 0.5 A g ⁻¹	S1
TBN-Car-CMP	18.90 F g ⁻¹ at 0.5 A g ⁻¹	S1
TBN-Car-CMP/SWCNT	53 at 0.5 A g ⁻¹	S1
H-THAQ	15 F g ⁻¹ at 1 A g ⁻¹	S2
THAQ/rGO (2:1)	76 F g ⁻¹ at 1 A g ⁻¹	S2
Pure AQ	42 F g ⁻¹ at 1 A g ⁻¹	S3
DAAQ-TFP COF	48 F g ⁻¹ at 0.1 A g ⁻¹	S4
TPA-COF-1	51.3 F g ⁻¹ at 0.2 A g ⁻¹	S5
TPA-COF-2	14.4 F g ⁻¹ at 0.2 A g ⁻¹	S5
TPA-COF-3	5.1 F g ⁻¹ at 0.2 A g ⁻¹	S5
TPT-COF-4	2.4 F g ⁻¹ at 0.2 A g ⁻¹	S5
TPT-COF-5	0.34 F g ⁻¹ at 0.2 A g ⁻¹	S5
TPT-COF-6	0.24 F g ⁻¹ at 0.2 A g ⁻¹	S5
Car-TPA COF	13.6 F g ⁻¹ at 0.2 A g ⁻¹	S6
Car-TPP COF	14.5 F g ⁻¹ at 0.2 A g ⁻¹	S6
Car-TPT COF	17.4 F g ⁻¹ at 0.2 A g ⁻¹	S6
TBN-BSU CMP	70 F g ⁻¹ at 0.5 A g ⁻¹	S7
Py-BSU CMP	38 F g ⁻¹ at 0.5 A g ⁻¹	S7
TPE-DDSQ-POIP	22 F g ⁻¹ at 1 A g ⁻¹	S8
Car-DDSQ-POIP	23 F g ⁻¹ at 1 A g ⁻¹	S8
CuTAPP-CMP/CNTs-1	70 F g ⁻¹ at 1.0 A g ⁻¹	S9
CuTAPP-CMP/CNTs-2	31 F g ⁻¹ at 1.0 A g ⁻¹	S9
CoPc/CNTs	31.5 F g ⁻¹ at 1.0 A g ⁻¹	S10
CoPc-CMP	13.8 F g ⁻¹ at 1.0 A g ⁻¹	S10
MWCNT@SACMP	549 F g ⁻¹ at 1.0 A g ⁻¹	S11

pNTCDA-TPAT	217.4 F g ⁻¹ at 0.5 A g ⁻¹	S12
PTPA@MWNT-4	410 F g ⁻¹ at 0.5 A g ⁻¹	S13
CNT@TFA-COF-3	338 F g ⁻¹ at 1 A g ⁻¹	S14

References

- [S1] M. M. Samy, M. G. Mohamed, A. F. M. El-Mahdy, T. H. Mansoure, K. C. W. Wu and S. W. Kuo, High-Performance Supercapacitor Electrodes Prepared From Dispersions of Tetrabenzonaphthalene-Based Conjugated Microporous Polymers and Carbon Nanotubes. *ACS Appl. Mater. Interfaces* 2021, **13**, 51906–51916. doi.org/10.1021/acsami.1c05720.
- [S2] L. Xu, R. Shi, H. Li, C. Han, M. Wu, C. P. Wong, F. Kang and B. Li, Pseudocapacitive anthraquinone modified with reduced graphene oxide for flexible symmetric all-solid-state supercapacitors, *Carbon*, 2018, **127**, 459-468. doi.org/10.1016/j.carbon.2017.11.003.
- [S3] B. Guo, Y. Yang, Z. Hu, Y. An, Q. Zhang, X. Yang, X. Wang and H. Wu, Redox-active organic molecules functionalized nitrogen-doped porous carbon derived from metal-organic framework as electrode materials for supercapacitor, *Electrochim. Acta*, 2017, **223**, 74–84. doi.org/10.1016/j.electacta.2016.12.012.
- [S4] C. R. DeBlase, K. E. Silberstein, T. T. Truong, H. D. Abruña and W. R. Dichtel, β -Ketoenamine-Linked Covalent Organic Frameworks Capable of Pseudocapacitive Energy Storage. *J. Am. Chem. Soc.*, 2013, **135**, 16821.
- [S5] A. F. M. EL-Mahdy, C. H. Kuo, A. Alshehri, C. Young, Y. Yamauchi, J. Kim and S. W. Kuo, Strategic design of triphenylamine- and triphenyltriazine-based two-dimensional covalent organic frameworks for CO₂ uptake and energy storage, *J. Mater. Chem. A*, 2018, **6**, 19532–19541. doi.org/10.1039/C8TA04781B
- [S6] A. F. M. El-Mahdy, C. Young, J. Kim, J. You, Y. Yamauchi and S. W. Kuo, Hollow Microspherical and Microtubular [3+3] Carbazole-Based Covalent Organic Frameworks and Their Gas and Energy Storage Applications. *ACS Appl. Mater. Interfaces* 2019, **11**, 9343–9354.

- [S7] M. G. Mohamed, S. Y. Chang, M. Ejaz, M. M. Samy, A. O. Mousa and S. W. Kuo, Design and Synthesis of Bisulfone-Linked Two-Dimensional Conjugated Microporous Polymers for CO₂ Adsorption and Energy Storage. *Molecules* 2023, **28**, 3234. <https://doi.org/10.3390/molecules28073234>.
- [S8] M. G. Mohamed, W. C. Chen, A. F. M. EL-Mahdy and S. W. Kuo, Porous organic/inorganic polymers based on double-decker silsesquioxane for high-performance energy storage, *J. Polym. Res.* 2021, **28**, 219. doi.org/10.1007/s10965-021-02579-x.
- [S9] L. Mei, J. C. Wei and Q. Duan, Construction of copper porphyrin-linked conjugated microporous polymer/carbon nanotube composite as flexible electrodes for supercapacitors. *J. Mater. Sci. Mater. Electron.* 2021, **32**, 24953–24963. doi.org/10.1007/s10854-021-06952-w.
- [S10] L. Mei, X. Cui, Q. Duan, Y. Li, X. Lv and H. G. Wang, Metal Phthalocyanine Linked Conjugated Microporous Polymer Hybridized with Carbon Nanotubes as a High-Performance Flexible Electrode for Supercapacitors. *Int. J. Hydrogen Energy*, 2020, **45**, 22950-22958. doi.org/10.1016/j.ijhydene.2020.06.208.
- [S11] W. Lyu, C. Yan, Z. Chen, J. Chen, H. Zuo, L. Teng, H. Liu, L. Wang and Y. Liao, Spirobifluorene-Based Conjugated Microporous Polymer-Grafted Carbon Nanotubes for Efficient Supercapacitive Energy Storage. *ACS Appl. Energy Mater.* 2022, **5**, 3706–3714. <https://doi.org/10.1021/acsaem.2c00151>.
- [S12] Y. Dai, Y. Wang, H. Xu, X. Li, X. Yan and X. Xu, Structure, morphology and energy storage properties of imide conjugated microporous polymers with different cores and the corresponding composites with CNT. *Electrochim. Acta* 2023, **441**, 141820. <https://doi.org/10.1016/j.electacta.2023.141820>.
- [S13] H. Zuo, J. Duan, B. Lyu, W. Lyu, Y. Li, X. Mei and Y. Liao, Carbon Nanotube Template-Assisted Synthesis of Conjugated Microporous Polytriphenylamine with High Porosity for Efficient

Supercapacitive Energy Storage. *Macromol. Rapid Commun.* 2023, 2300238.
<https://doi.org/10.1002/marc.202300238>.

[S14] L. Liu, D. Cui, S. Zhang, W. Xie, C. Yao and Y. Xu, Integrated carbon nanotube and triazine-based covalent organic framework composites for high capacitance performance. *Dalton Trans.*, 2023, **52**, 2762–2769. <https://doi.org/10.1039/D2DT03910A>.